

FastGS: Training 3D Gaussian Splatting in 100 Seconds

Shiwei Ren* Tianci Wen* Yongchun Fang† Biao Lu
NanKai University

renshiwei, wentc, lubiao@mail.nankai.edu.cn, fangyc@nankai.edu.cn

<https://fastgs.github.io>

| Static Scene Reconstruction | | | | | | Dynamic Reconstruction | | | Surface Reconstruction | | | |
|-----------------------------|--------------|--------------|----------|---------|--------|------------------------|-------|----------|------------------------|-------|-------|---------|
| Ground Truth | Speedy-Splat | FastGS(ours) | Time/min | PSNR/dB | N_GS/M | Deformable-3DGS | PGSR | Time/min | PSNR/dB | F1 | F0.62 | |
| | | | 12.22 | 21.59 | 0.11 | 21.55 | 26.86 | 0.15 | 34.17 | 24.92 | 1.71 | F1:0.62 |
| | | | 3.03 | 22.50 | 0.37 | 7.63 | 30.20 | 0.07 | 15.27 | 25.07 | 0.33 | F1:0.60 |

Figure 1. We propose FastGS, a general acceleration framework for 3D Gaussian Splatting (3DGS) that significantly reduces training time without sacrificing rendering quality. In static scenes, our method completes training on the Tanks & Temples *train* scene within 100 seconds. Furthermore, our method achieves 2.82× and 2.24× faster training for dynamic and surface reconstruction, respectively.

Abstract

The dominant 3D Gaussian splatting (3DGS) acceleration methods fail to properly regulate the number of Gaussians during training, causing redundant computational time overhead. In this paper, we propose FastGS, a novel, simple, and general acceleration framework that fully considers the importance of each Gaussian based on multi-view consistency, efficiently solving the trade-off between training time and rendering quality. We innovatively design a densification and pruning strategy based on multi-view consistency, dispensing with budgeting mechanism. Extensive experiments on Mip-NeRF 360, Tanks & Temples, and Deep Blending datasets demonstrate that our method significantly outperforms the state-of-the-art (SOTA) methods in training speed, achieving a 3.32× training acceleration and comparable rendering quality compared with DashGaussian on the Mip-NeRF 360 dataset and a 15.45× acceleration compared with vanilla 3DGS on the Deep Blending dataset. We demonstrate that FastGS exhibits strong generality, delivering 2-7× training acceleration across various tasks, including dynamic scene reconstruction, surface reconstruction, sparse-view reconstruction, large-scale re-

construction and simultaneous localization and mapping.

1. Introduction

Novel view synthesis (NVS) is a fundamental problem in computer vision and graphics, with broad applications in augmented reality [48], virtual reality [41] and autonomous driving [39]. Neural Radiance Field (NeRF) [27] methods model scenes as continuous volumetric functions and render photorealistic views, but require hours of training per scene. Recently, 3D Gaussian Splatting (3DGS) [17] has achieved rendering quality comparable to NeRF while offering significantly faster training and rendering speed. It models 3D scenes via explicit Gaussian primitives and employs a tile-based rasterizer. Benefiting from its efficiency, 3DGS has been successfully applied to a wide range of tasks, including dynamic scene reconstruction, surface reconstruction and simultaneous localization and mapping (SLAM). However, a major bottleneck in its current practical application is the extended training time, which often requires tens of minutes per scene, hindering user-friendly deployment.

*Equal contribution.

†Corresponding author.

A detailed analysis of the vanilla 3DGS training pipeline reveals two primary limitations: (1) its adaptive density control (ADC) of Gaussians often introduces a large number of redundant Gaussians, and (2) inefficiencies in the vanilla 3DGS rendering pipeline. While recent works [9, 11, 12, 25] have significantly optimized the rendering pipeline, ADC remains a major area for improvement.

ADC in vanilla 3DGS comprises two main components. The first is Gaussian densification, which clones or splits a Gaussian based on its positional gradient. The second is Gaussian pruning, which removes Gaussians with low opacity or oversized scales. Existing 3DGS acceleration methods [4, 6, 8, 10, 12, 22, 25, 28, 36] have introduced improvements to ADC. One direction of improvement focuses on designing mechanisms to constrain Gaussian densification, aiming to minimize the growth of redundant Gaussians. For example, Taming-3DGS [25] employs a budget-constrained optimization to control Gaussian growth. Similarly, DashGaussian [4] leverages an adaptive Gaussian primitive budgeting method to maintain continuous densification throughout training. The other direction involves refining the pruning strategy to accelerate training by deleting a greater number of redundant Gaussians. For example, Speedy-Splat [12] applies a soft pruning strategy during densification and a hard pruning strategy afterward.

One major drawback of these methods is the limited effectiveness of their densification and pruning strategies, which fail to maintain rendering quality while avoiding excessive Gaussian redundancy, resulting in an inefficient representation, as illustrated in Fig. 2. This indicates that their Gaussian control strategies are suboptimal. Based on our observations, some densification and pruning methods [1, 4, 10, 17–19, 34, 44] do not leverage multi-view consistency, while others [12, 13, 25, 47] exploit it suboptimally. Specifically, they enforce multi-view consistency merely through Gaussian-related scores, which we argue is insufficient. It may lead to the excessive growth of redundant Gaussians that provide only marginal improvements to the rendering quality from a few viewpoints while contributing little to others. On one hand, for certain densification methods such as Taming-3DGS [25], Gaussian importance is considered across views. However, it fully relies on Gaussian-related scores rather than their actual contribution to rendering quality, resulting in weak multi-view constraints and leading to redundancy. Moreover, it lacks a dedicated redesign of the pruning strategy. On the other hand, for some pruning methods such as Speedy-Splat [12], multi-view information is also considered, but it uses the gradients of Gaussian rather than evaluating each Gaussian’s contribution to multi-view rendering quality. This indirect enforcement of multi-view consistency leads to significant degradation in rendering quality.

To address the above issues, we propose FastGS, a new,

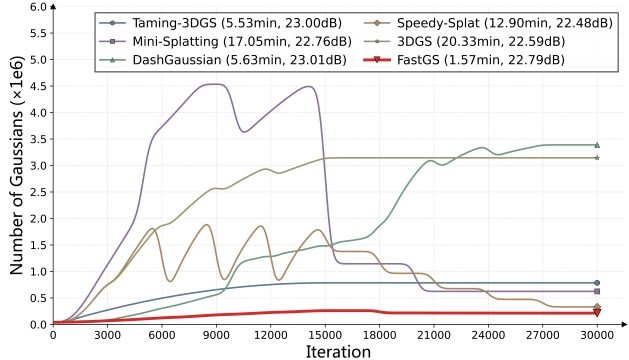


Figure 2. **Gaussian Count Over Training Iterations.** Benefiting from the efficient VCD and VCP strategies, FastGS maintains the smallest number of Gaussians throughout the entire training.

simple, and general 3DGS acceleration framework, capable of training a scene within 100 seconds while maintaining comparable rendering quality, as shown in Fig. 1. In fact, nearly every Gaussian primitive participates in rendering the same region across multiple viewpoints. Our insight is similar to the concept behind bundle adjustment in traditional 3D reconstruction, where each 3D Gaussian should maintain multi-view consistency. This implies that the 3D Gaussian should enhance rendering quality across multiple views of the same region. Therefore, we introduce a multi-view consistent densification (VCD) strategy, which uses a multi-view reconstruction quality importance score to evaluate whether a Gaussian contributes beneficially to the improvement of multi-view rendering quality. Based on the same idea, we propose a multi-view consistent pruning (VCP) strategy, which removes redundant Gaussians that are useless to multi-view rendering quality. Notably, because VCD and VCP accurately identifies which Gaussians need to be densified or pruned, our method does not require a budget mechanism, making it applicable to other tasks easily. To summarize our contributions,

1. **New, simple and general framework** for 3DGS acceleration that can train a scene within 100 seconds while achieving the comparable rendering quality.
2. **Efficient densification and pruning strategy** strictly controls the addition and removal of each Gaussian based on its contribution to multi-view reconstruction quality, greatly accelerating the training process.
3. **State-of-the-Art Performance** on extensive experiments across Mip-NeRF 360, Tanks & Temples, and Deep Blending datasets. Our method outperforms the state-of-the-art (SOTA) approaches in training efficiency while maintaining comparable rendering quality.
4. **Strong generality** across various tasks, such as dynamic scene reconstruction, surface reconstruction, sparse-view reconstruction, large-scale reconstruction and SLAM. FastGS achieves an average 2–7× training speedup.

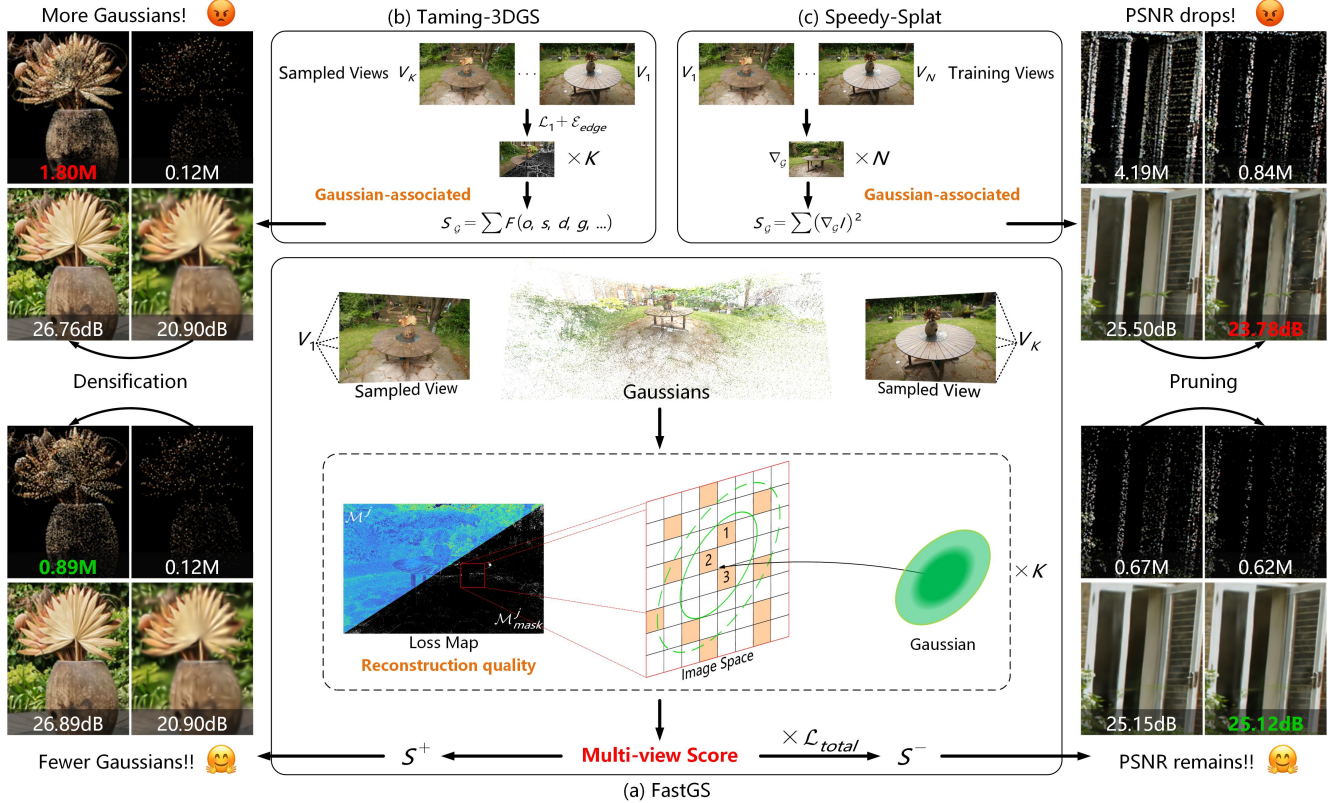


Figure 3. **The pipeline of FastGS.** (a) We redesign the ADC of the vanilla 3DGS [17] based on multi-view consistency. To accurately assess the importance of each Gaussian, we sample training views and generate the corresponding per-pixel L1 loss maps. For each sampled view, a multi-view score is computed for each Gaussian by counting the number of high-error pixels within its 2D footprint, which is subsequently used to guide Gaussian densification and pruning. (b) Taming-3DGS [25] primarily computes the importance score based on Gaussian-associated properties across sampled views. (c) Speedy-Splat [12] computes the Gaussian score by accumulating Gaussian-associated Hessian approximations across all training views. We visualize the densification results from 0.5K to 15K iterations without any pruning on the far left of the figure, and the pruning results after removing Gaussians at the 6K-th iteration on the far right.

2. Related Work

In this section, we review related works that focus on accelerating both the training and inference of 3DGS [17].

Gaussian densification. A key bottleneck of 3DGS is the excessive Gaussians that significantly slow down the training process. Recent works [4, 18, 19, 25, 33, 44, 47] attempt to address this issue by refining the densification strategy to control the primitive count. Specifically, 3DGS-MCMC [18] adopts a Monte Carlo strategy for Gaussian densification. Taming-3DGS [25] employs a budgeting mechanism to control Gaussian growth, primarily computing Gaussian scores based on Gaussian-associated properties. DashGaussian [4] also uses a budgeting method to guide Gaussian densification. Nevertheless, they still require millions of Gaussians to maintain rendering quality, resulting in heavy optimization overhead.

Gaussian Pruning. Besides modifying densification, some methods [1, 7, 8, 10, 12, 13, 28, 34] achieve accelera-

tion by designing pruning strategies to remove a large number of Gaussians. Some of them design importance scores according to Gaussian properties to guide pruning, discarding less critical Gaussians [1, 7, 10]. Mini-Splatting [8] removes a large number of Gaussians through a simplification strategy based on intersection preserving and sampling. PUP 3DGS [13] and Speedy-Splat [12] remove Gaussians by computing a Gaussian-associated Hessian approximation across all training views. Nonetheless, some of them fail to fully remove redundant Gaussians, while others remove many Gaussians at the cost of significantly degraded rendering quality.

Other Methods. Some works focus on optimizing 3DGS rasterization or optimization strategies. Taming-3DGS [25] replaces per-pixel with per-splat parallel backpropagation, which significantly speeds up the optimization process and serves as a strong baseline for subsequent research. StopThePop [31], FlashGS [9], and Speedy-sSplat [12] use precise tile intersection to reduce Gaussian-tile pairs and

accelerate rasterization. 3DGS-LM [15] replaces Adam with Levenberg-Marquardt for faster convergence, and 3DGS² [22] achieves near second-order convergence via prioritized per-kernel updates.

3. Background: 3D Gaussian Splatting

3DGS models a scene as an explicit point-based representation composed of a set of anisotropic 3D Gaussians:

$$\{\mathcal{G}_i(\mathbf{x}) = \exp(-\frac{1}{2}(\mathbf{x} - \boldsymbol{\mu}_i)^\top \boldsymbol{\Sigma}_{i_{3D}}^{-1}(\mathbf{x} - \boldsymbol{\mu}_i))\}_{i=1}^N. \quad (1)$$

To construct this representation, a sparse point cloud obtained from SfM is used to initialize the positions of Gaussian primitives. Each primitive \mathcal{G}_i is parameterized by mean $\boldsymbol{\mu}_i \in \mathbb{R}^3$, rotation $r_i \in \mathbb{R}^4$, scale $s_i \in \mathbb{R}^3$, opacity $\sigma_i \in [0, 1)$, and color coefficients $\mathbf{c}_i \in \mathbb{R}^{16 \times 3}$ represented in view-dependent spherical harmonics (SH). The rotation and scale together define the covariance matrix as

$$\boldsymbol{\Sigma}_{i_{3D}} = R_i S_i S_i^\top R_i^\top. \quad (2)$$

To render from a given camera viewpoint, all 3D Gaussians need to be projected into the 2D image plane. Given a viewing transformation W , the covariance matrix in camera coordinates is computed as

$$\boldsymbol{\Sigma}'_{i_{2D}} = J W \boldsymbol{\Sigma}_{i_{3D}} J^\top W^\top, \quad (3)$$

where J denotes the Jacobian of the affine approximation of the projective transformation. The projected 3D Gaussian is then approximated as a 2D elliptical Gaussian on the image plane, with covariance $\boldsymbol{\Sigma}'_{i_{2D}}$ obtained by marginalizing $\boldsymbol{\Sigma}'_{i_{3D}}$ along the viewing direction. Each 2D Gaussian contributes to pixels within its footprint using α -blending: given Gaussians $\{\mathcal{G}_i\}_{i=1}^N$ sorted by depth, the accumulated color of pixel p is computed as

$$C(p) = \sum_{i \in N} c_i \alpha_i \prod_{j=1}^{i-1} (1 - \sigma_j), \quad \alpha_i = \sigma_i \mathcal{G}'_i(p), \quad (4)$$

where

$$\mathcal{G}'_i(p) = \exp\left(-\frac{1}{2}(p - \boldsymbol{\mu}_{i_{2D}})^\top \boldsymbol{\Sigma}'_{i_{2D}}^{-1}(p - \boldsymbol{\mu}_{i_{2D}})\right), \quad (5)$$

with $\boldsymbol{\mu}_{i_{2D}}$ and $\boldsymbol{\Sigma}'_{i_{2D}}$ denoting the mean and covariance of the projected 2D Gaussian, respectively.

4. FastGS

4.1. Overview

The framework of our method is shown in Fig. 3. We initialize 3D Gaussians using SfM point clouds, and train the 3DGS model on multi-view images. The addition and removal of 3D Gaussians are controlled via the proposed

multi-view consistent densification and pruning strategies. As illustrated in Fig. 3b and Fig. 3c, Taming-3DGS [25] and Speedy-Splat [12] also estimate Gaussian scores from multiple views, for densification and pruning respectively. However, both rely on Gaussian-associated scores to control the number of Gaussians rather than considering each Gaussian’s contribution to multi-view rendering quality. This suboptimal use of multi-view information results in redundancy for Taming-3DGS [25] and degraded rendering quality for Speedy-Splat [12]. In contrast, as illustrated in Fig. 3a, our method evaluates the importance of each Gaussian based on multi-view reconstruction quality, rather than its properties. Furthermore, our method leverages multi-view consistency for both densification and pruning, which will be detailed in Sections Sec. 4.2 and Sec. 4.3. To further improve rasterization efficiency, Sec. 4.4 introduces the Compact Box (CB) we use.

4.2. Multi-view Consistent Densification

The vanilla 3DGS [17] densifies Gaussians solely based on the gradient magnitude in the image space, which leads to a large number of redundant Gaussians. Other densification methods [4, 8, 44] also generate millions of Gaussians, leading to inefficiency. We argue that the redundancy arises because these methods fail to rigorously determine from multiple views whether a Gaussian needs densification. As illustrated in Fig. 3b, Taming-3DGS [25] considers multi-view consistency during densification. However, it primarily computes the score based on Gaussian-associated properties (e.g., opacity, scale, depth and gradient) rather than their actual contribution to the rendering quality, making it difficult to enforce strict multi-view consistency for a Gaussian. This also leads to redundancy, as visualized on the left of Fig. 3b. Moreover, the computation of its score is complex and relatively inefficient. To address these issues, we propose a new, simple densification strategy VCD based on multi-view consistency. As illustrated in Fig. 3a, it computes the average number of high-error pixels in each Gaussian’s 2D footprint across sampled views, where high-error pixels are identified solely from the per-pixel L1 loss between the ground truth and the rendering. As shown in the left of Fig. 3a, VCD achieves comparable rendering quality with fewer Gaussians, thereby greatly avoiding redundancy. We then detail how VCD is implemented.

Given K camera views $V = \{v^j\}_{j=1}^K$, randomly sampled from the training views, together with their corresponding ground-truth images $G = \{g^j\}_{j=1}^K$ and rendered images $R = \{r^j\}_{j=1}^K$. For each view v^j , we compute the error between the rendered color $r_{u,v}^{j,c}$ and the ground-truth color $g_{u,v}^{j,c}$ at pixel (u, v) :

$$e_{u,v}^j = \frac{1}{C} \sum_{c=1}^C |r_{u,v}^{j,c} - g_{u,v}^{j,c}|, \quad (6)$$

where $c \in \{1, 2, \dots, C\}$ denotes the color channel. We then construct the loss map $\mathcal{M}^j \in \mathbb{R}^{W \times H}$ from the per-pixel errors:

$$\mathcal{M}^j = \{\hat{e}_{u,v}^j\}_{u=0,v=0}^{W-1,H-1}, \quad (7)$$

where each $\hat{e}_{u,v}^j$ is obtained via min-max normalization:

$$\hat{e}_{u,v}^j = \frac{e_{u,v}^j - \min_{u,v}(e_{u,v}^j)}{\max_{u,v}(e_{u,v}^j) - \min_{u,v}(e_{u,v}^j) + \varepsilon}, \quad (8)$$

with ε being a small constant for numerical stability. A threshold τ is then applied to \mathcal{M}^j to identify pixel p_h with high reconstruction error, forming a mask:

$$\mathcal{M}_{\text{mask}}^j = \mathbb{I}(\mathcal{M}^j > \tau), \quad (9)$$

where pixels P with $\mathcal{M}_{\text{mask}}^j(u, v) = 1$ indicate regions of poor reconstruction quality.

Next, we need to find the Gaussian primitives associated with these high-error pixels. For each 3D Gaussian primitive \mathcal{G}_i , we project it onto the 2D image space to obtain its 2D footprint Ω_i . We then use an indicator function $\mathbb{I}(\mathcal{M}_{\text{mask}}^j(p) = 1)$ to determine whether a pixel has high error. We compute an importance score s_i^+ for each Gaussian primitive, which accumulates the number of high-error pixels contained in the 2D footprint across all sampled views and then averages the accumulated value:

$$s_i^+ = \frac{1}{K} \sum_{j=1}^K \sum_p^{\Omega_i} \mathbb{I}(\mathcal{M}_{\text{mask}}^j(p) = 1), \quad (10)$$

where a higher s_i^+ indicates that the Gaussian consistently lies in high-error regions across multiple views, thus suggesting it as a candidate for densification. A Gaussian primitive \mathcal{G}_i is selected for densification if its importance score s_i^+ exceeds a predefined threshold τ_+ , indicating that it contributes significantly to under-reconstructed regions across multiple views. Notably, we can efficiently determine the number of high-error pixels within the 2D footprint directly from the forward pass of the render.

4.3. Multi-view Consistent Pruning

The vanilla 3DGS [17] removes Gaussians with low opacity or overly large scale but cannot effectively address redundancy. Recent pruning strategies [1, 7, 8] similarly fail to eliminate redundancy and can even significantly degrade rendering quality. In all cases, they do not determine Gaussian redundancy based on multi-view consistency. As illustrated in Fig. 3c, Speedy-Splat [12] computes the pruning score by accumulating Gaussian-associated Hessian approximations across all training views rather than capturing each Gaussian’s true contribution to multi-view rendering

quality. Hence, it leads to degraded rendering quality due to its indirect use of multi-view consistency, as visualized on the right of Fig. 3c. To remove truly redundant Gaussians, we propose a new, simple pruning strategy VCP based on multi-view consistency. As illustrated in Fig. 3a, similar to VCD, it evaluates the score according to each Gaussian’s impact on multi-view reconstruction quality. As shown on the right of Fig. 3a, VCP removes a significant number of redundant Gaussians while preserving rendering quality. We then detail how VCP is implemented.

Specifically, for each view $v^j \in V$, we compute the photometric loss between the rendered image r^j and the corresponding ground-truth image g^j :

$$E_{\text{photo}}^j = (1 - \lambda)L_1^j + \lambda(1 - L_{\text{SSIM}}^j), \quad (11)$$

where L_1^j and L_{SSIM}^j denote the mean absolute error and the structural similarity loss over the entire image, respectively. Since the photometric loss provides a reliable indicator of reconstruction fidelity, we incorporate it with Eq. (10) to derive the pruning score for each Gaussian primitive \mathcal{G}_i :

$$s_i^- = \mathcal{N} \left(\sum_{j=1}^K \left(\sum_p^{\Omega_i} \mathbb{I}(\mathcal{M}_{\text{mask}}^j(p) = 1) \right) \cdot E_{\text{photo}}^j \right), \quad (12)$$

where $\mathcal{N}(\cdot)$ denotes a min-max normalization function. Here, s_i^- can be interpreted as a quantitative measure of the contribution of Gaussian primitive \mathcal{G}_i to the degradation of the overall rendering quality. A Gaussian primitive \mathcal{G}_i is selected for pruning if its importance score s_i^- exceeds a predefined threshold τ_- , indicating that it has relatively low contribution to rendering quality across multiple views.

4.4. Compact Box

During the preprocessing stage of rasterization, the vanilla 3DGS [17] uses the 3-sigma rule to obtain 2D ellipses, generating many Gaussian-tile pairs that introduce computational redundancy and reduce rendering efficiency. Speedy-Splat [12] partially addresses this with precise tile intersect, yet we observe that some 2D Gaussians still have negligible impact on pixels in certain tiles. To further reduce unnecessary pairs, we propose Compact Box, which prunes Gaussian-tile pairs with minimal contribution based on their Mahalanobis distance from the Gaussian center, thereby accelerating rendering while maintaining quality. Details are provided in the supplementary material.

4.5. Optimization

Same as the vanilla 3DGS [17], we optimize the learnable parameters with respect to the L1 loss over rendered pixel colors, combined with the SSIM term [37] $\mathcal{L}_{\text{SSIM}}$. The total supervision is defined as:

$$\mathcal{L} = (1 - \lambda)\mathcal{L}_1 + \lambda(1 - \mathcal{L}_{\text{SSIM}}). \quad (13)$$

Table 1. **Quantitative comparisons with existing 3DGS fast optimization methods.** With FastGS, the training of 3DGS can be completed within **100 seconds** on average, while achieving comparable rendering quality to the other methods. Best results are marked as **best score**, **second best score** and **third best score**. Time is reported in minutes.

| Method | Mip-NeRF 360 [2] | | | | | | Deep Blending [14] | | | | | | Tanks & Temples [21] | | | | | |
|---------------------|------------------|--------------|--------------|--------------|-------------------|------------|--------------------|--------------|--------------|--------------|-------------------|------------|----------------------|--------------|--------------|--------------|-------------------|------------|
| | Time↓ | PSNR↑ | SSIM↑ | LPIPS↓ | N _{GS} ↓ | FPS↑ | Time↓ | PSNR↑ | SSIM↑ | LPIPS↓ | N _{GS} ↓ | FPS↑ | Time↓ | PSNR↑ | SSIM↑ | LPIPS↓ | N _{GS} ↓ | FPS↑ |
| 3DGS [17] | 20.93 | 27.53 | 0.813 | 0.221 | 2.63M | 146 | 19.77 | 29.71 | 0.903 | 0.241 | 2.46M | 158 | 11.34 | 23.71 | 0.850 | 0.170 | 1.57M | 195 |
| 3DGS-accel [17, 25] | 10.94 | 27.52 | 0.813 | 0.221 | 2.63M | 188 | 8.87 | 29.74 | 0.903 | 0.242 | 2.46M | 230 | 6.96 | 23.85 | 0.850 | 0.170 | 1.57M | 252 |
| Mini-Splatting [8] | 17.71 | 27.33 | 0.821 | 0.217 | 0.53M | 564 | 13.35 | 29.99 | 0.907 | 0.244 | 0.56M | 624 | 9.06 | 23.46 | 0.844 | 0.181 | 0.30M | 756 |
| Speedy-splat [12] | 13.38 | 26.91 | 0.781 | 0.295 | 0.30M | 552 | 10.75 | 29.42 | 0.898 | 0.272 | 0.25M | 664 | 6.32 | 23.38 | 0.816 | 0.242 | 0.18M | 691 |
| Taming-3DGS [25] | 5.36 | 27.48 | 0.794 | 0.261 | 0.68M | 221 | 3.06 | 29.50 | 0.894 | 0.278 | 0.29M | 352 | 2.71 | 23.89 | 0.833 | 0.214 | 0.32M | 379 |
| DashGaussian [4] | 6.38 | 27.73 | 0.817 | 0.217 | 2.40M | 154 | 4.16 | 29.65 | 0.906 | 0.246 | 1.94M | 208 | 4.28 | 24.00 | 0.853 | 0.178 | 1.21M | 240 |
| FastGS-20k (Ours) | 1.32 | 27.35 | 0.793 | 0.268 | 0.39M | 568 | 0.88 | 29.93 | 0.901 | 0.274 | 0.22M | 687 | 0.95 | 23.81 | 0.835 | 0.216 | 0.25M | 632 |
| FastGS (Ours) | 1.92 | 27.54 | 0.796 | 0.264 | 0.38M | 584 | 1.28 | 30.03 | 0.901 | 0.270 | 0.22M | 714 | 1.32 | 24.15 | 0.839 | 0.210 | 0.24M | 655 |
| FastGS-Big (Ours) | 3.59 | 27.93 | 0.820 | 0.216 | 1.16M | 472 | 2.00 | 30.12 | 0.907 | 0.242 | 0.65M | 607 | 2.03 | 24.39 | 0.855 | 0.175 | 0.54M | 569 |

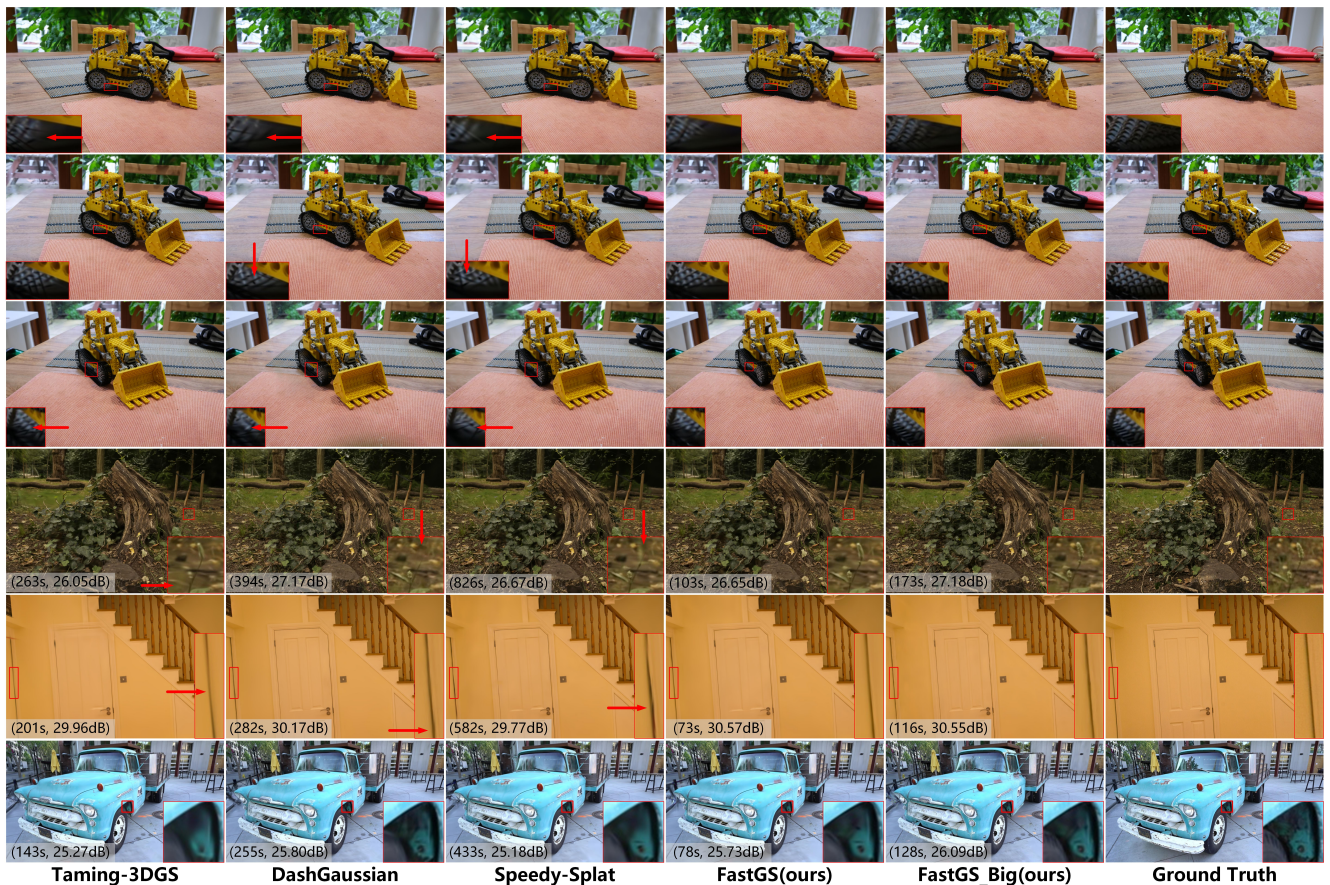


Figure 4. **Qualitative results of Tab. 1.** We present qualitative results on the “kitchen” and “stump” scenes from the Mip-NeRF 360 dataset [2], the “playroom” scene from the Deep Blending dataset [5], and the “truck” scene from the Tanks&Temples dataset [21].

5. Experiments

5.1. Experimental Setup

Datasets. Same as vanilla 3DGS [17], we conduct experiments on three real-world datasets: Mip-NeRF 360 [2], Deep-Blending [14], and Tanks & Temples [21]. For other challenging tasks, we evaluate dynamic scene reconstruc-

tion on D-NeRF [30], NeRF-DS [42], and Neu3D [23] datasets. Tanks & Temples [21], LLFF [26], BungeeNeRF [40] and Replica [35] are respectively used for surface reconstruction, sparse-view reconstruction, large-scale reconstruction and SLAM.

Metrics. To evaluate the performance, we report commonly used metrics for novel view rendering quality, including

Table 2. **Quantitative results of accelerating various 3DGS backbones using FastGS.** By integrating FastGS into different backbones, the training speed achieves a 2-14 \times improvement. Time is reported in minutes.

| Method | Mip-NeRF 360 [2] | | | | | | Deep Blending [14] | | | | | | Tanks & Temples [21] | | | | | |
|---------------------|-------------------|-----------------|-----------------|--------------------|--------------------|----------------|--------------------|-----------------|-----------------|--------------------|--------------------|----------------|----------------------|-----------------|-----------------|--------------------|--------------------|----------------|
| | Time \downarrow | PSNR \uparrow | SSIM \uparrow | LPIPS \downarrow | $N_{GS}\downarrow$ | FPS \uparrow | Time \downarrow | PSNR \uparrow | SSIM \uparrow | LPIPS \downarrow | $N_{GS}\downarrow$ | FPS \uparrow | Time \downarrow | PSNR \uparrow | SSIM \uparrow | LPIPS \downarrow | $N_{GS}\downarrow$ | FPS \uparrow |
| 3DGS [17] | 20.93 | 27.53 | 0.813 | 0.221 | 2.63M | 146 | 19.77 | 29.71 | 0.903 | 0.241 | 2.46M | 158 | 11.34 | 23.71 | 0.850 | 0.170 | 1.57M | 195 |
| +Ours | 9.18 | 27.54 | 0.796 | 0.264 | 0.39M | 504 | 9.60 | 30.09 | 0.901 | 0.270 | 0.22M | 618 | 4.93 | 24.24 | 0.840 | 0.209 | 0.24M | 586 |
| Mip-Splatting [45] | 26.20 | 27.89 | 0.837 | 0.176 | 3.98M | 224 | 23.94 | 29.35 | 0.899 | 0.241 | 3.48M | 219 | 14.57 | 23.77 | 0.856 | 0.158 | 2.36M | 300 |
| +Ours | 2.98 | 27.95 | 0.828 | 0.208 | 0.83M | 606 | 1.74 | 29.68 | 0.899 | 0.274 | 0.20M | 698 | 2.01 | 24.18 | 0.843 | 0.200 | 0.36M | 729 |
| Scaffold-GS [24] | 18.37 | 27.70 | 0.812 | 0.226 | 0.57M | 194 | 13.31 | 30.09 | 0.905 | 0.256 | 0.18M | 307 | 9.83 | 24.09 | 0.851 | 0.175 | 0.26M | 261 |
| +Ours | 5.06 | 27.68 | 0.809 | 0.220 | 0.30M | 281 | 2.82 | 30.00 | 0.900 | 0.267 | 0.08M | 423 | 3.77 | 24.15 | 0.849 | 0.180 | 0.14M | 332 |
| 3DGS-accel [17, 25] | 10.94 | 27.52 | 0.813 | 0.221 | 2.63M | 188 | 8.87 | 29.74 | 0.903 | 0.242 | 2.46M | 230 | 6.96 | 23.85 | 0.850 | 0.170 | 1.57M | 252 |
| +Ours | 1.92 | 27.54 | 0.796 | 0.264 | 0.38M | 584 | 1.28 | 30.03 | 0.901 | 0.270 | 0.22M | 714 | 1.32 | 24.15 | 0.839 | 0.210 | 0.24M | 655 |

Table 3. **Quantitative results of dynamic scene reconstruction.** Our method achieves an average 2.60 \times training speed-up.

| Dataset | Method | Time \downarrow | PSNR \uparrow | SSIM \uparrow | LPIPS \downarrow | $N_{GS}\downarrow$ | FPS \uparrow |
|--------------|----------------------|-------------------|-----------------|-----------------|--------------------|--------------------|----------------|
| NeRF-DS [42] | Deformable-3DGS [43] | 7.86 | 23.83 | 0.851 | 0.180 | 0.13M | 103 |
| | +Ours | 2.75 | 23.90 | 0.854 | 0.176 | 0.03M | 484 |
| Neu3D [23] | Deformable-3DGS [43] | 25.11 | 27.78 | 0.902 | 0.158 | 0.20M | 73 |
| | +Ours | 8.70 | 30.25 | 0.919 | 0.140 | 0.08M | 172 |

PSNR, SSIM [38], and LPIPS [46]. In addition, training efficiency and model compactness are assessed by reporting the total training time (in minutes), the final number of Gaussians, and the rendering speed (FPS).

Implementation Details. All methods, including ours and the other compared approaches, are trained for 30K iterations using the Adam [20] optimizer. For our approach, we set $K = 10$ and $\lambda = 0.2$ in all experiments. In the base setting, densification is performed every 500 iterations until the 15,000-th iteration. To ensure fairness, all experiments are conducted with an NVIDIA RTX 4090 GPU, and all comparison methods are implemented using their official code. The default configuration of FastGS is 3DGS-accel [17, 25] with the proposed VCD, VCP, and CB. To achieve extreme training acceleration, the rendering quality of our method is not the highest. Therefore, we provide a variant, **FastGS-Big**, which achieves both the highest rendering quality and the fastest training speed, where densification is executed once every 100 iterations. Further details are in the supplementary material.

5.2. Comparison with Fast Optimization Methods

Baselines. We adopt 3DGS-accel [17, 25] as our baseline which preserves the original 3DGS [17] pipeline and incorporates the efficient per-splat parallel backpropagation proposed by Taming-3DGS [25]. Beyond this baseline, we further conduct comparisons against several recent SOTA acceleration techniques, including DashGaussian [4], Mini-Splatting [8], Speedy-Splat [12], and Taming-3DGS [25], which represent complementary advances in accelerating training from different perspectives.

Table 4. **Quantitative results of surface reconstruction.** Our method achieves a 2-7 \times training speed-up.

| Dataset | Method | Time \downarrow | PSNR \uparrow | SSIM \uparrow | LPIPS \downarrow | $N_{GS}\downarrow$ | FPS \uparrow | F1 \uparrow |
|----------------------|----------|-------------------|-----------------|-----------------|--------------------|--------------------|----------------|---------------|
| Tanks & Temples [21] | PGSR [3] | 32.92 | 24.20 | 0.857 | 0.149 | 1.56M | 87 | 0.57 |
| | +Ours | 15.73 | 24.37 | 0.845 | 0.190 | 0.40M | 210 | 0.55 |
| Mip-NeRF 360 [2] | PGSR [3] | 74.70 | 27.22 | 0.832 | 0.183 | 3.79M | 45 | - |
| | +Ours | 11.68 | 27.23 | 0.813 | 0.240 | 0.49M | 202 | - |

Quantitative Results. As shown in Tab. 1, FastGS achieves the fastest training with comparable rendering quality. On average, a scene can be trained within 100 seconds, and the fastest case takes only 77 seconds. This benefit comes from our effective multi-view consistent densification and pruning strategies. Speedy-Splat [12] fails to fully consider multi-view consistency during pruning, leading to a significant drop in rendering quality. Taming3DGS [25] applies weak multi-view consistency constraints, resulting in excessive Gaussian growth and slower training. The current SOTA, DashGaussian [4], achieves high rendering quality yet lacks an effective pruning strategy to remove redundant Gaussians. Its scene optimization still retains several million Gaussians, limiting training speed. In contrast, our variant FastGS-Big surpasses DashGaussian [4] by more than 0.2 dB in rendering quality, reduces training time by over 43.7%, and cuts the number of Gaussians by more than half. These results demonstrate the superiority of our multi-view consistent densification and pruning strategies.

We visualize the results of Tab. 1 in Fig. 4, providing a detailed comparison of reconstructed scenes across different methods. Our method FastGS achieves comparable rendering quality without losing any details. In addition, our variant FastGS-Big reconstructs scenes more accurately, with more precise geometric structures under the multi-view consistency constraint.

5.3. Generality of FastGS

Baselines. Deformable-3DGS [43], PGSR [3], DropGaussian [29], OctreeGS [32] and Photo-SLAM [16] are selected as the backbones for dynamic scene reconstruction, surface

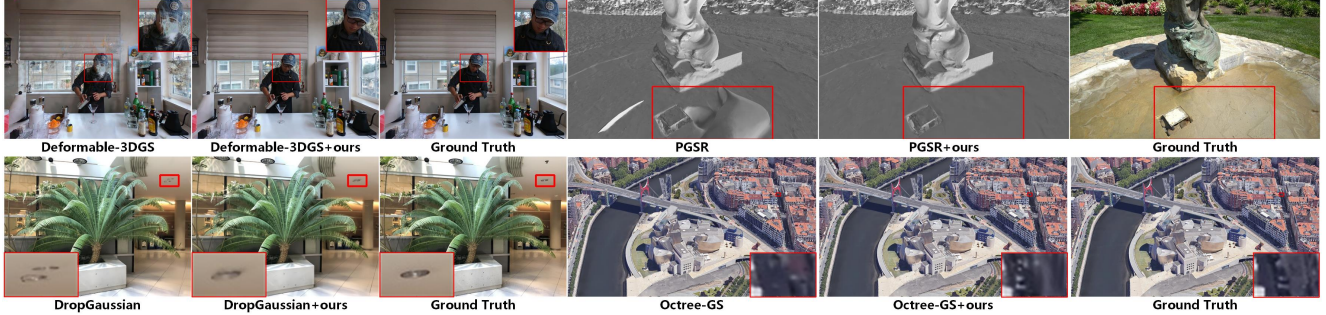


Figure 5. **Visualization results on four representative tasks.** We present the rendered results of the “coffee-martini”, “Ignatius”, “fern”, and “bilbao” scenes from the Neu3D [23], Tanks and Temples [21], LLFF [26], and BungeeNeRF [40] datasets, respectively.

reconstruction, sparse-view reconstruction, large-scale reconstruction and SLAM, respectively.

Enhancing Backbone. Due to the simplicity of our framework, it can be easily applied to other 3DGS backbones with different optimizers [25], representation primitives [24], or additional filters [45]. As shown in Tab. 2, Our method achieves 2–14× faster training and an average 77.46% reduction in the number of Gaussians while maintaining the same rendering quality. This demonstrates the strong generality of our approach, which we attribute to the fact that multi-view consistency is fundamental to 3D reconstruction tasks. The implementation details for each backbone are provided in the supplementary material.

Enhancing Various Tasks. We further test several SOTA methods combined with our framework across these tasks. As shown in Tab. 3 and Tab. 4, our method improves the training speed of all baselines by 2-7× while preserving rendering quality. We visualize some results in Fig. 5. This improvement demonstrates the strong generality of our approach. We argue that this benefits from the multi-view consistency, which is fundamental to various reconstruction tasks. More results are provided in the supplementary material and we will open-source our code.

5.4. Ablation Study

We adopt 3DGS-accel [17, 25] as our baseline and systematically evaluate the contribution of each proposed module. By adding each component individually, we analyze its impact on both reconstruction quality and training efficiency, providing insights into the effectiveness of our design.

Multi-View Consistent Densification. We first evaluate the effect of the densification strategy VCD. As shown in Tab. 5, VCD achieves nearly 3× faster training without any loss in reconstruction quality. This is because our Gaussian addition is guided by stricter multi-view consistency, which prevents the addition of redundant Gaussians. Tab. 5 further validates this by showing that with VCD, the number of Gaussians is reduced by 80%. This ablation study demonstrates the effectiveness of VCD for accelerating training.

Multi-View Consistent Pruning. Next, we evaluate the ef-

Table 5. **Ablation studies over the proposed methods of FastGS.** Experiments are performed on the Mip-NeRF 360 dataset [2] with 3DGS-accel [17, 25] as the baseline.

| Method | Time↓ | PSNR↑ | SSIM↑ | LPIPS↓ | N_{GS} ↓ | FPS↑ |
|------------|-------------|--------------|--------------|--------------|--------------|------------|
| 3DGS-accel | 10.94 | 27.52 | 0.813 | 0.221 | 2.63M | 188 |
| +VCD. | 3.60 | 27.58 | 0.798 | 0.260 | 0.51M | 228 |
| +VCP. | 5.60 | 27.53 | 0.812 | 0.228 | 1.87M | 292 |
| +CB. | 10.08 | 27.51 | 0.810 | 0.219 | 2.76M | 325 |
| Full | 1.92 | 27.54 | 0.796 | 0.264 | 0.38M | 584 |

fectiveness of VCP. As shown in Tab. 5, adding VCP shortens the training time by 48.8% and reduces the number of Gaussians by 28.9%, without sacrificing rendering quality. This is because our method effectively removes redundant Gaussians while preserving those critical for scene reconstruction. The strict multi-view consistency evaluation for each deleted Gaussian ensures this effectiveness, demonstrating that VCP is highly effective.

Compact Box. Finally, we evaluate the effectiveness of Compact Box. As shown in Tab. 5, adding CB shortens the training time by 7.8% while achieving the comparable rendering quality. This demonstrates that CB can accelerate training without degrading reconstruction quality.

5.5. Discussions and Limitations

We identify two additional directions to further accelerate training. (1) Our current bottleneck lies in the need for 30k optimization steps. Designing faster-converging optimization strategies that require fewer steps could significantly improve training speed. (2) Another bottleneck is that training starts from scratch with COLMAP initialization. Developing a general feed-forward NVS model and fine-tuning on its results could also greatly shorten training time.

6. Conclusion

This paper introduces a novel, simple, and general acceleration framework FastGS. We propose multi-view consistent Gaussian densification and pruning strategies that prevent redundant Gaussians and significantly accelerate

3DGS training. Extensive experiments demonstrate the effectiveness of our view-consistency design. Our method achieves the fastest training speed among all SOTA methods while maintaining comparable rendering quality. The results also demonstrate strong generality of FastGS, greatly reducing training time across various tasks such as dynamic scene reconstruction, surface reconstruction, and so on.

References

- [1] Muhammad Salman Ali, Maryam Qamar, Sung-Ho Bae, and Enzo Tartaglione. Trimming the fat: Efficient compression of 3d gaussian splats through pruning. *arXiv preprint arXiv:2406.18214*, 2024. 2, 3, 5
- [2] Jonathan T Barron, Ben Mildenhall, Dor Verbin, Pratul P Srinivasan, and Peter Hedman. Mip-nerf 360: Unbounded anti-aliased neural radiance fields. In *Proceedings of the IEEE/CVF conference on computer vision and pattern recognition*, pages 5470–5479, 2022. 6, 7, 8
- [3] Danpeng Chen, Hai Li, Weicai Ye, Yifan Wang, Weijian Xie, Shangjin Zhai, Nan Wang, Haomin Liu, Hujun Bao, and Guofeng Zhang. Pgsr: Planar-based gaussian splatting for efficient and high-fidelity surface reconstruction. *IEEE Transactions on Visualization and Computer Graphics*, 2024. 7
- [4] Youyu Chen, Junjun Jiang, Kui Jiang, Xiao Tang, Zhihao Li, Xianming Liu, and Yinyu Nie. Dashgaussian: Optimizing 3d gaussian splatting in 200 seconds. In *Proceedings of the Computer Vision and Pattern Recognition Conference*, pages 11146–11155, 2025. 2, 3, 4, 6, 7
- [5] Kangle Deng, Andrew Liu, Jun-Yan Zhu, and Deva Ramanan. Depth-supervised nerf: Fewer views and faster training for free. In *Proceedings of the IEEE/CVF conference on computer vision and pattern recognition*, pages 12882–12891, 2022. 6
- [6] Xiaobin Deng, Changyu Diao, Min Li, Ruohan Yu, and Du-anqing Xu. Efficient density control for 3d gaussian splatting. *arXiv preprint arXiv:2411.10133*, 2024. 2
- [7] Zhiwen Fan, Kevin Wang, Kairun Wen, Zehao Zhu, Dejie Xu, Zhangyang Wang, et al. Lightgaussian: Unbounded 3d gaussian compression with 15x reduction and 200+ fps. *Advances in neural information processing systems*, 37: 140138–140158, 2024. 3, 5
- [8] Guangchi Fang and Bing Wang. Mini-splatting: Representing scenes with a constrained number of gaussians. In *European Conference on Computer Vision*, pages 165–181. Springer, 2024. 2, 3, 4, 5, 6, 7
- [9] Guofeng Feng, Siyan Chen, Rong Fu, Zimu Liao, Yi Wang, Tao Liu, Boni Hu, Linning Xu, Zhilin Pei, Hengjie Li, et al. Flashgs: Efficient 3d gaussian splatting for large-scale and high-resolution rendering. In *Proceedings of the Computer Vision and Pattern Recognition Conference*, pages 26652–26662, 2025. 2, 3
- [10] Sharath Girish, Kamal Gupta, and Abhinav Shrivastava. Eagles: Efficient accelerated 3d gaussians with lightweight encodings. In *European Conference on Computer Vision*, pages 54–71. Springer, 2024. 2, 3
- [11] Hao Gui, Lin Hu, Rui Chen, Mingxiao Huang, Yuxin Yin, Jin Yang, Yong Wu, Chen Liu, Zhongxu Sun, Xueyang Zhang, et al. Balanced 3dgs: Gaussian-wise parallelism rendering with fine-grained tiling. *arXiv preprint arXiv:2412.17378*, 2024. 2
- [12] Alex Hanson, Allen Tu, Geng Lin, Vasu Singla, Matthias Zwicker, and Tom Goldstein. Speedy-splat: Fast 3d gaussian splatting with sparse pixels and sparse primitives. In *Proceedings of the Computer Vision and Pattern Recognition Conference*, pages 21537–21546, 2025. 2, 3, 4, 5, 6, 7
- [13] Alex Hanson, Allen Tu, Vasu Singla, Mayuka Jayawardhana, Matthias Zwicker, and Tom Goldstein. Pup 3d-gs: Principled uncertainty pruning for 3d gaussian splatting. In *Proceedings of the Computer Vision and Pattern Recognition Conference*, pages 5949–5958, 2025. 2, 3
- [14] Peter Hedman, Julien Philip, True Price, Jan-Michael Frahm, George Drettakis, and Gabriel Brostow. Deep blending for free-viewpoint image-based rendering. *ACM Transactions on Graphics (ToG)*, 37(6):1–15, 2018. 6, 7
- [15] Lukas Höllein, Aljaž Božič, Michael Zollhöfer, and Matthias Nießner. 3dgs-lm: Faster gaussian-splatting optimization with levenberg-marquardt. *arXiv preprint arXiv:2409.12892*, 2024. 4
- [16] Huajian Huang, Longwei Li, Cheng Hui, and Sai-Kit Yeung. Photo-slam: Real-time simultaneous localization and photo-realistic mapping for monocular, stereo, and rgb-d cameras. In *Proceedings of the IEEE/CVF Conference on Computer Vision and Pattern Recognition*, 2024. 7
- [17] Bernhard Kerbl, Georgios Kopanas, Thomas Leimkühler, and George Drettakis. 3d gaussian splatting for real-time radiance field rendering. *ACM Transactions on Graphics*, 42(4), 2023. 1, 2, 3, 4, 5, 6, 7, 8
- [18] Shakiba Kheradmand, Daniel Rebain, Gopal Sharma, Weiwei Sun, Yang-Che Tseng, Hossam Isack, Abhishek Kar, Andrea Tagliasacchi, and Kwang Moo Yi. 3d gaussian splatting as markov chain monte carlo. *Advances in Neural Information Processing Systems*, 37:80965–80986, 2024. 3
- [19] Sieun Kim, Kyungjin Lee, and Youngki Lee. Color-cued efficient densification method for 3d gaussian splatting. In *Proceedings of the IEEE/CVF Conference on Computer Vision and Pattern Recognition*, pages 775–783, 2024. 2, 3
- [20] Diederik P Kingma. Adam: A method for stochastic optimization. *arXiv preprint arXiv:1412.6980*, 2014. 7
- [21] Arno Knapitsch, Jaesik Park, Qian-Yi Zhou, and Vladlen Koltun. Tanks and temples: Benchmarking large-scale scene reconstruction. *ACM Transactions on Graphics (ToG)*, 36(4):1–13, 2017. 6, 7, 8
- [22] Lei Lan, Tianjia Shao, Zixuan Lu, Yu Zhang, Chenfanfu Jiang, and Yin Yang. 3dgs2: Near second-order converging 3d gaussian splatting. In *Proceedings of the Special Interest Group on Computer Graphics and Interactive Techniques Conference Conference Papers*, pages 1–10, 2025. 2, 4
- [23] Tianye Li, Mira Slavcheva, Michael Zollhoefer, Simon Green, Christoph Lassner, Changil Kim, Tanner Schmidt, Steven Lovegrove, Michael Goesele, Richard Newcombe, et al. Neural 3d video synthesis from multi-view video. In *Proceedings of the IEEE/CVF conference on computer vision and pattern recognition*, pages 5521–5531, 2022. 6, 7, 8

- [24] Tao Lu, Mulin Yu, Linning Xu, Yuanbo Xiangli, Limin Wang, Dahua Lin, and Bo Dai. Scaffold-gs: Structured 3d gaussians for view-adaptive rendering. In *Proceedings of the IEEE/CVF Conference on Computer Vision and Pattern Recognition*, pages 20654–20664, 2024. 7, 8
- [25] Saswat Subhajyoti Mallick, Rahul Goel, Bernhard Kerbl, Markus Steinberger, Francisco Vicente Carrasco, and Fernando De La Torre. Taming 3dgs: High-quality radiance fields with limited resources. In *SIGGRAPH Asia 2024 Conference Papers*, pages 1–11, 2024. 2, 3, 4, 6, 7, 8
- [26] Ben Mildenhall, Pratul P Srinivasan, Rodrigo Ortiz-Cayon, Nima Khademi Kalantari, Ravi Ramamoorthi, Ren Ng, and Abhishek Kar. Local light field fusion: Practical view synthesis with prescriptive sampling guidelines. *ACM Transactions on Graphics (TOG)*, 38(4):1–14, 2019. 6, 8
- [27] Ben Mildenhall, Pratul P Srinivasan, Matthew Tancik, Jonathan T Barron, Ravi Ramamoorthi, and Ren Ng. Nerf: Representing scenes as neural radiance fields for view synthesis. *Communications of the ACM*, 65(1):99–106, 2021. 1
- [28] Panagiotis Papanotakis, Georgios Kopanas, Bernhard Kerbl, Alexandre Lanvin, and George Drettakis. Reducing the memory footprint of 3d gaussian splatting. *Proceedings of the ACM on Computer Graphics and Interactive Techniques*, 7(1):1–17, 2024. 2, 3
- [29] Hyunwoo Park, Gun Ryu, and Wonjun Kim. Dropgaussian: Structural regularization for sparse-view gaussian splatting. In *Proceedings of the Computer Vision and Pattern Recognition Conference*, pages 21600–21609, 2025. 7
- [30] Albert Pumarola, Enric Corona, Gerard Pons-Moll, and Francesc Moreno-Noguer. D-nerf: Neural radiance fields for dynamic scenes. In *Proceedings of the IEEE/CVF conference on computer vision and pattern recognition*, pages 10318–10327, 2021. 6
- [31] Lukas Radl, Michael Steiner, Mathias Parger, Alexander Weinrauch, Bernhard Kerbl, and Markus Steinberger. Stopthepop: Sorted gaussian splatting for view-consistent real-time rendering. *ACM Transactions on Graphics (TOG)*, 43(4):1–17, 2024. 3
- [32] Kerui Ren, Lihan Jiang, Tao Lu, Mulin Yu, Linning Xu, Zhangkai Ni, and Bo Dai. Octree-gs: Towards consistent real-time rendering with lod-structured 3d gaussians. *arXiv preprint arXiv:2403.17898*, 2024. 7
- [33] Samuel Rota Bulò, Lorenzo Porzi, and Peter Kotschieder. Revising densification in gaussian splatting. In *European Conference on Computer Vision*, pages 347–362. Springer, 2024. 3
- [34] Muhammad Salman Ali, Sung-Ho Bae, and Enzo Tartaglione. ElmgS: Enhancing memory and computation scalability through compression for 3d gaussian splatting. *arXiv e-prints*, pages arXiv–2410, 2024. 2, 3
- [35] Julian Straub, Thomas Whelan, Lingni Ma, Yufan Chen, Erik Wijmans, Simon Green, Jakob J. Engel, Raul Mur-Artal, Carl Ren, Shobhit Verma, Anton Clarkson, Mingfei Yan, Brian Budge, Yajie Yan, Xiaqing Pan, June Yon, Yuyang Zou, Kimberly Leon, Nigel Carter, Jesus Briales, Tyler Gillingham, Elias Mueggler, Luis Pesqueira, Manolis Savva, Dhruv Batra, Hauke M. Strasdat, Renzo De Nardi, Michael Goesele, Steven Lovegrove, and Richard Newcombe. The Replica dataset: A digital replica of indoor spaces. *arXiv preprint arXiv:1906.05797*, 2019. 6
- [36] Xinzhe Wang, Ran Yi, and Lizhuang Ma. Adr-gaussian: Accelerating gaussian splatting with adaptive radius. In *SIGGRAPH Asia 2024 Conference Papers*, pages 1–10, 2024. 2
- [37] Zhou Wang, A.C. Bovik, H.R. Sheikh, and E.P. Simoncelli. Image quality assessment: from error visibility to structural similarity. *IEEE Transactions on Image Processing*, 13(4):600–612, 2004. 5
- [38] Zhou Wang, Alan C Bovik, Hamid R Sheikh, and Eero P Simoncelli. Image quality assessment: from error visibility to structural similarity. *IEEE transactions on image processing*, 13(4):600–612, 2004. 7
- [39] Zirui Wu, Tianyu Liu, Liyi Luo, Zhide Zhong, Jianteng Chen, Hongmin Xiao, Chao Hou, Haozhe Lou, Yuantao Chen, Runyi Yang, et al. Mars: An instance-aware, modular and realistic simulator for autonomous driving. In *CAAI International Conference on Artificial Intelligence*, pages 3–15. Springer, 2023. 1
- [40] Yuanbo Xiangli, Linning Xu, Xingang Pan, Nanxuan Zhao, Anyi Rao, Christian Theobalt, Bo Dai, and Dahua Lin. Bungeenerf: Progressive neural radiance field for extreme multi-scale scene rendering. In *European conference on computer vision*, pages 106–122. Springer, 2022. 6, 8
- [41] Linning Xu, Vasu Agrawal, William Laney, Tony Garcia, Aayush Bansal, Changil Kim, Samuel Rota Bulò, Lorenzo Porzi, Peter Kotschieder, Aljaž Božič, et al. Vr-nerf: High-fidelity virtualized walkable spaces. In *SIGGRAPH Asia 2023 Conference Papers*, pages 1–12, 2023. 1
- [42] Zhiwen Yan, Chen Li, and Gim Hee Lee. Nerf-ds: Neural radiance fields for dynamic specular objects. In *Proceedings of the IEEE/CVF Conference on Computer Vision and Pattern Recognition*, pages 8285–8295, 2023. 6, 7
- [43] Ziyi Yang, Xinyu Gao, Wen Zhou, Shaohui Jiao, Yuqing Zhang, and Xiaogang Jin. Deformable 3d gaussians for high-fidelity monocular dynamic scene reconstruction. In *Proceedings of the IEEE/CVF conference on computer vision and pattern recognition*, pages 20331–20341, 2024. 7
- [44] Zongxin Ye, Wenyu Li, Sidun Liu, Peng Qiao, and Yong Dou. Absgs: Recovering fine details in 3d gaussian splatting. In *Proceedings of the 32nd ACM International Conference on Multimedia*, pages 1053–1061, 2024. 2, 3, 4
- [45] Zehao Yu, Anpei Chen, Binbin Huang, Torsten Sattler, and Andreas Geiger. Mip-splatting: Alias-free 3d gaussian splatting. In *Proceedings of the IEEE/CVF conference on computer vision and pattern recognition*, pages 19447–19456, 2024. 7, 8
- [46] Richard Zhang, Phillip Isola, Alexei A Efros, Eli Shechtman, and Oliver Wang. The unreasonable effectiveness of deep features as a perceptual metric. In *Proceedings of the IEEE conference on computer vision and pattern recognition*, pages 586–595, 2018. 7
- [47] Zheng Zhang, Wenbo Hu, Yixing Lao, Tong He, and Hengshuang Zhao. Pixel-gs: Density control with pixel-aware gradient for 3d gaussian splatting. In *European Conference on Computer Vision*, pages 326–342. Springer, 2024. 2, 3

- [48] Tinghui Zhou, Richard Tucker, John Flynn, Graham Fyffe, and Noah Snavely. Stereo magnification: Learning view synthesis using multiplane images. *arXiv preprint arXiv:1805.09817*, 2018. 1